Monthly Notices
of the
ROYAL ASTRONOMICAL SOCIETY

MNRAS **466,** 1462–1476 (2017)
Advance Access publication 2016 October 30

doi:10.1093/mnras/stw2777

Black hole growth and AGN feedback under clumpy accretion

C. DeGraf,[1,2]★ A. Dekel,[1] J. Gabor[3] and F. Bournaud[3]

[1]*Center for Astrophysics and Planetary Science, Racah Institute of Physics, The Hebrew University, Jerusalem 91904, Israel*
[2]*Institute of Astronomy and Kavli Institute for Cosmology, University of Cambridge, Madingley Road, Cambridge CB3 0HA, UK*
[3]*CEA-Saclay, F-91190 Gif-sur-Yvette, France*

Accepted 2016 October 26. Received 2016 October 25; in original form 2014 December 4

ABSTRACT

High-resolution simulations of supermassive black holes in isolated galaxies have suggested the importance of short (∼10 Myr) episodes of rapid accretion caused by interactions between the black hole and massive dense clouds within the host. Accretion of such clouds could potentially provide the dominant source for black hole growth in high-z galaxies, but it remains unresolved in cosmological simulations. Using a stochastic subgrid model calibrated by high-resolution isolated galaxy simulations, we investigate the impact that variability in black hole accretion rates has on black hole growth and the evolution of the host galaxy. We find this clumpy accretion to more efficiently fuel high-redshift black hole growth. This increased mass allows for more rapid accretion even in the absence of high-density clumps, compounding the effect and resulting in substantially faster overall black hole growth. This increased growth allows the black hole to efficiently evacuate gas from the central region of the galaxy, driving strong winds up to ∼2500 km s^{-1}, producing outflows ∼10 × stronger than the smooth accretion case, suppressing the inflow of gas on to the host galaxy, and suppressing the star formation within the galaxy by as much as a factor of 2. This suggests that the proper incorporation of variability is a key factor in the co-evolution between black holes and their hosts.

Key words: black hole physics – methods: numerical – galaxies: active – galaxies: haloes – quasars: general.

1 INTRODUCTION

Observations suggest that supermassive black holes are to be found at the centres of most galaxies (Kormendy & Richstone 1995), and properties of the black hole and the host galaxies are strongly correlated (Magorrian et al. 1998; Ferrarese & Merritt 2000; Gebhardt et al. 2000; Tremaine et al. 2002; Novak, Faber & Dekel 2006; Graham & Driver 2007; Cattaneo et al. 2009; Kormendy & Ho 2013; McConnell & Ma 2013). These correlations suggest that the growth of a black hole and the evolution of its host galaxy influence one another. As such, black holes provide a means to better understand the evolution of galaxies, and may provide a key aspect to this evolution. One of the most common explanations for this correlation is that the quasar feedback from the central black hole may influence the host galaxy (e.g. Burkert & Silk 2001; Granato et al. 2004; Sazonov, Ostriker & Sunyaev 2004; Churazov et al. 2005; Di Matteo, Springel & Hernquist 2005; Kawata & Gibson 2005; Springel et al. 2005; Begelman, Volonteri & Rees 2006; Bower et al. 2006; Croton et al. 2006; Ciotti & Ostriker 2007; Hopkins, Richards & Hernquist 2007; Malbon et al. 2007; Sijacki et al. 2007; Sijacki, Springel & Haehnelt 2009; DeGraf et al. 2012b; Di Matteo et al. 2012; Dubois et al. 2013a; Dubois et al. 2013b). This feedback energy may be sufficient to unbind gas within the galaxy, driving strong outflows (Silk & Rees 1998; Wyithe & Loeb 2003). Observations of galactic-scale outflows have been made (e.g. Fabian et al. 2006; Spoon et al. 2013; Veilleux et al. 2013; Cicone et al. 2014), showing that such outflows certainly exist. Furthermore, there is evidence that the strongest velocities are located in the centralmost region of the galaxy (Rupke, Veilleux & Sanders 2005; Rupke & Veilleux 2011), possibly suggesting that the driving force behind them is indeed a centrally located Active Galactic Nucleus (AGN) rather than more widely distributed feedback sources such as stars and supernovae.

Driving these large-scale outflows necessarily requires a large energy output from the AGN, which in turn requires a significant source of gas which can reach the black hole at the Galactic Centre. The angular momentum loss required for this infall can pose a challenge. One of the more commonly posed explanations is that a gas-rich merger can drive gas towards the black hole. Theoretical work suggests that mergers should drive significant AGN activity (e.g. Hernquist 1989; Di Matteo et al. 2005; Hopkins et al. 2005a,b; Hopkins et al. 2008; Johansson, Burkert & Naab 2009; Debuhr et al. 2010; Debuhr, Quataert & Ma 2011) and some observations support this (Ellison et al. 2011). However, there have also been

★ E-mail: cdegraf@ast.cam.ac.uk

many studies which find that, although mergers may drive some AGN activity, the majority of AGN are found in isolated galaxies (Schmitt 2001; Grogin et al. 2005; Coldwell & Lambas 2006; Gabor et al. 2009; Georgakakis et al. 2009; Cisternas et al. 2011; Kocevski et al. 2012), suggesting that an alternate, secular mechanism may be the primary driving force in AGN activity. One of the main drivers of AGN activity at high redshift is believed to be cold flows: high-density streams of low angular momentum cold gas flowing along the cosmic web, whose high density and low temperature allow efficient penetration of haloes to the innermost regions where they can continually fuel black hole growth (Di Matteo et al. 2012; Dubois et al. 2012). In addition, theoretical work has suggested that in high-z, gas-rich galaxies, violent disc instabilities can drive gas inflow and produce dense clumps of gas which can be driven in towards the Galactic Centre (Dekel, Sari & Ceverino 2009; Ceverino, Dekel & Bournaud 2010; Bournaud et al. 2011; Mandelker et al. 2014), which may be a primary cause of AGN activity (Bournaud et al. 2012) and provides a means of rapidly growing black holes even in the absence of cold streams.

In a companion paper, Gabor & Bournaud (2013) used high-resolution (6 pc) simulations to show that accretion on to black holes in gas-rich galaxies can be highly variable, with strong bursts of accretion caused by dense infalling gas clouds. These accretion events were found to generate strong outflows, but without significant effect on the host galaxy (Gabor & Bournaud 2014), at least over short ($\sim$100 Myr) time-scales and in the absence of cosmological gas flows and mergers. Similarly, Novak, Ostriker & Ciotti (2011) used 2D simulations to show that cool shells of gas would fragment, with the fragmentation leading to bursts of accretion and an overall higher accretion rate. In this paper, we investigate the impact of periodic bursts of accretion on the growth of black holes and the corresponding effect they have on the host galaxy in a cosmological context, in which the black holes grow by several orders of magnitude (spanning both quiescent AGN phases and stronger quasar phases of extended Eddington growth). We use zoom-in simulations to achieve $\sim$100 pc resolution for galaxies in a cosmological environment, utilizing a stochastic subgrid model to incorporate the accretion of unresolved high-density gas clouds. We investigate how, in the context of cosmological gas inflow and galaxy mergers, the inclusion of periodic, high-accretion events affects black hole growth, and the impact this has on the host galaxy morphology and star formation rate, and on galactic gas inflow and outflow.

The paper is organized as follows. In Section 2, we describe the simulations used and detail the subgrid model for the periodic accretion bursts. In Section 3, we investigate the impact of these periodic accretion bursts on black hole growth. In Section 4, we show how AGN feedback from these accretion bursts can affect the host, specifically host morphology (Section 4.1), gas properties of the host (Section 4.2), and gas inflows/outflows (Section 4.3). In Section 5, we compare the impact at earlier times, providing a more direct comparison to the high-resolution isolated galaxy run. Finally, we summarize our results in Section 6.

2 METHOD

2.1 RAMSES CODE

For this work, we ran cosmological zoom-in simulations using the Adaptive Mesh Refinement (AMR) code RAMSES (Teyssier 2002), which uses particles (acting as collisionless fluid) to model dark matter and stars, while gas is modelled by solving the hydrodynamic equations on a cubic grid of cells which vary in size. This code incorporates cooling, star formation, stellar feedback, and black holes. Cooling is performed as a sink term in the thermal energy of the gas. We allow gas to cool to a minimum temperature floor of $T_{\rm th} = 10^4$ K, together with a density-dependent temperature floor to keep the local Jeans length above four cell-sizes, with a polytropic equation of state $T = T_{\rm th}(\rho/\rho_{\rm th})^{\gamma-1}$ with $\gamma = 2$, thereby preventing artificial fragmentation (see e.g. Truelove et al. 1997). A uniform UV background (neglecting local sources) heats the gas according to the model of Haardt & Madau (1996), using $z_{\rm reion} = 8.5$.

Star formation is performed in gas cells above the critical density $n_H > 0.1$ cm^{-3}. The star formation rate is $\dot{\rho} = \epsilon_* \rho_{\rm gas}/t_{\rm ff}$, where $\rho_{\rm gas}$ is the gas density in the cell, $t_{\rm ff} = (3\pi/32 G\rho_{\rm gas})^{1/2}$ is the local free-fall time of the gas, and $\epsilon_* = 0.01$ is the star formation efficiency (Kennicutt 1998; Krumholz & Tan 2007). New star particles are then formed stochastically according to the star formation rate of the cell (Rasera & Teyssier 2006), initially given the position and velocity of the host cell, but uncoupled from the cell. Supernova feedback is modelled by depositing 10 per cent of a star particles initial mass into the local cell 10 Myr after formation. The energy released is 10^{50} erg per M$_\odot$ per M$_\odot$ of stars which go supernova. The energy is deposited thermally on to the gas, and cooling within the cell in which the energy is deposited is delayed by 2 Myr to prevent overcooling of the gas (following approaches taken by e.g. Stinson et al. 2006; Teyssier et al. 2013; Gabor & Bournaud 2014).

We use the same supermassive black hole prescription as Gabor & Bournaud (2013) (see also Dubois et al. 2012). Black holes are represented as sink particles, seeded into cells whose densities surpass $n_H > 1\,{\rm cm}^{-3}$, with an initial mass of $M_{\rm seed} = 10^5\,{\rm M}_\odot$. Rather than representing the initial formation of an unresolved seed, this mass is broadly consistent with multiple mechanisms for seed formation, e.g. collapse of PopIII stars (e.g. Bromm & Larson 2004; Yoshida et al. 2006) or direct collapse of massive gas clouds (e.g. Bromm & Loeb 2003; Begelman et al. 2006), followed by sufficient growth to reach $M_{\rm seed}$. We also prevent black holes from forming within 25 kpc of another BH, thereby preventing multiple BHs from forming within the same galaxy. Once seeded, the black hole grows through gas accretion and BH–BH mergers. Gas accretion is modelled as

$$\dot{M}_{\rm BH} = (4\alpha\pi G^2 M_{\rm BH}^2 \rho)/(c_s^2 + v_{\rm rel}^2)^{3/2} \quad (1)$$

(Hoyle & Lyttleton 1939; Bondi & Hoyle 1944; Bondi 1952), where ρ is the gas density, c_s is the sound speed of the gas, $v_{\rm rel}$ is the velocity of the black hole relative to the gas (calculated within a sphere of $4r_{\rm min}$, where $r_{\rm min}$ is the minimum resolution element of the simulation), and $\alpha = (\rho/\rho_0)^2$ for $\rho > \rho_0$ and $\alpha = 1$ for $\rho < \rho_0$ (Booth & Schaye 2009). To prevent unphysically high accretion rates, we cap $\dot{M}_{\rm BH}$ at the Eddington limit

$$\dot{M}_{\rm edd} = (4\pi G M_{\rm BH} m_p)/(\epsilon_r \sigma_T c) \quad (2)$$

(Eddington 1916), where m_p is the mass of a proton, σ_T is the Thomson scattering cross-section, c is the speed of light, and ϵ_r is the radiative efficiency for the accreting gas, assumed to be 0.1 (Shakura & Sunyaev 1973).

Black hole feedback is accomplished using a thermal feedback model, depositing $\dot{E}_{\rm BH} = \epsilon_f \epsilon_r \dot{M}_{\rm BH}$ ($\epsilon_f = 0.15$ is the feedback efficiency, selected to reproduce the scaling relations between the black hole and the host galaxy; see Dubois et al. 2012) on to the gas within $4r_{\rm min}$ of the BH. To prevent instantaneous overcooling of the gas (which will tend to happen at low temperatures where the cooling rate is high enough), we only deposit this energy if it is sufficient to heat the gas to at least 10^7 K, otherwise the energy is stored until this threshold can be reached (Booth & Schaye 2009).

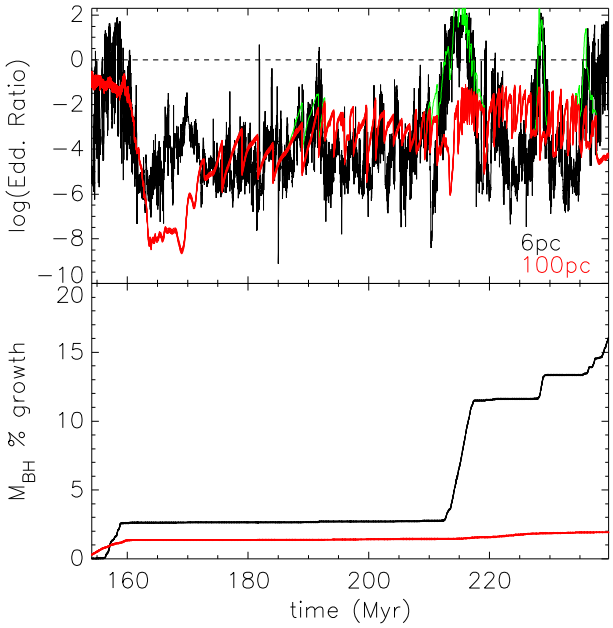

Figure 1. Resolution dependence of black hole growth. Top: Eddington fraction ($\dot{M}_{\rm BH}/\dot{M}_{\rm edd}$) for black hole in isolated galaxy simulation using 6 pc resolution (black) and 100 pc resolution (red). Dashed line shows the Eddington limit. Green curve shows the 100 pc run with added Gaussian curves for bursts of accretion (used for stochastic subgrid model; see Section 2.2). Bottom: black hole growth (as a percentage of its initial mass) over the course of the simulations. Lowering the resolution smooths out the highest peaks and leads to significantly lower BH growth.

To prevent unphysically high temperatures, if the thermal feedback is sufficient to heat the gas in excess of 5×10^9 K, the injection region is iteratively expanded until the resulting temperature will be below this level.

2.2 Clumpy-accretion model

The key modification to the black hole treatment in this paper is the incorporation of unresolved high-density gas clouds.

Gabor & Bournaud (2013) found that the accretion of high-density clouds of gas could be the dominant factor is black hole growth (at least among gas-rich, high-z galaxies), based on isolated galaxy simulations with 6 pc resolution. Because these clouds of gas are only ∼100–300 pc in radius, they remain unresolved in the majority of cosmological simulations. To investigate the effect of using resolution more typical for cosmological runs, we re-ran the M4f50 run from Gabor & Bournaud (2013) at the lower resolution of 100 pc. In Fig. 1, we show the comparison between the 6 pc resolution (black) and 100 pc resolution (red) runs. On few-timestep scales, the high-resolution simulation exhibits more variation, as may be expected. In addition to the general variability, we note two main differences. First, the high-resolution simulation has several periods of high accretion on the order of 5–10 Myr. Secondly, in the absence of these accretion events, the low-resolution simulation tends to accrete more rapidly, by a factor of ∼2.5–3. This increased accretion in the low-resolution run is seen most clearly in the upper panel of Fig. 1 between 190–210 and 220–235 Myr, where the red (low resolution) is clearly significantly higher than the black (high resolution), except during a clump accretion event. In the bottom panel of Fig. 1, we show the black hole growth for both the high- (black) and low- (red) resolution runs. Here, we see that the short accretion events contributing the majority of the black hole growth in the high-resolution simulation are missed in the low-resolution run, leaving the black hole at a much smaller final mass.

Given the importance of these high-density gas clouds on the black hole growth, we incorporate a subgrid prescription to the accretion rate to boost the accretion as if a high-density gas cloud were able to be resolved. We use a simple stochastic prescription for our model. For any timestep in which a black hole is not already undergoing a burst of accretion, we allow for a new event to begin with a probability of $p_{\rm burst}$. Each such event causes the accretion rate of the black hole to increase following a Gaussian pattern, with a characteristic time-scale ($\sigma_{\rm burst}$) and amplitude ($A_{\rm burst}$). We use the high- and low-resolution runs (shown in Fig. 1) to calibrate the values of these parameters. We do this by fitting Gaussians to the rate of increase in the ratio between the accretion rates of the two simulations, finding four events which occur during the comparison period. From this, we incorporate four possible clump accretion events to our simulation, which each occurs once in the 85 Myr high-resolution run. These four events occur with amplitude $A_{\rm burst} = 26.5$, 6.22, 5.56, and4.66, with time-scales of $\sigma_{\rm burst} = 1.83$, 1.3, 0.4, and 1.5 Myr, respectively. To account for the slower accretion during the smooth period (i.e. in the absence of a dense clump), the smooth accretion decreased by a factor of ∼2.6 (matching the discrepancy in Fig. 1). The model calibration is intended to give the lower resolution cosmological run a periodicity comparable to that of the high-resolution run which fully resolves high-density clouds. Given the limited sample size of a single isolated galaxy over a relatively short time-scale (for cosmological runs), this will not be a completely accurate parametrization, particularly since it does not depend on the various properties of the host. In particular, we expect the formation of dense gas clumps to occur in gas-rich galaxies, but such formation may be minimal (if at all) in gas-poor galaxies. Indeed, this is found in Gabor & Bournaud (2013), which explicitly showed that gas-poor galaxies did not form the dense clumps found in gas-rich galaxies. For this paper, we investigate the impact which periodic accretion can have on the black hole growth and on the host in a galaxy where such clump formation occurs, for which this parametrization is sufficient. We also note that the galaxy in our simulation has a gas fraction in excess of 50 per cent throughout the run, making the gas-rich run from Gabor & Bournaud (2013) the appropriate one to use here. Having demonstrated the importance of including such variability in this work, we note that a full parameter study of how accretion of high-density clumps depends on host properties will be needed. This will require a full suite of high-resolution isolated galaxy simulations to study clump formation as a function of galaxy properties, such as gas-fraction, galactic scaleheight, Star Formation Rate (SFR), merger history, etc. Such a suite of simulations is beyond the scope of this work, however, and is thus left for a follow-up project. We also note the possibility that runs with resolution beyond the 6 pc used in the isolated galaxy may exhibit slightly different behaviour. However, since the clumps in the isolated galaxy are well resolved (typically on the order of ∼100 pc), we do not expect significant impact from higher resolution.

2.3 Zoom-in simulations

For this paper, we run a set of zoom-in simulations within a 10 Mpc box. We assume a lambda cold dark matter cosmology with cosmological parameters consistent with Planck Collaboration XVI (2013): $\Omega_\Lambda = 0.68$, $\Omega_{\rm m} = 0.32$, $\Omega_b = 0.05$, and $H_0 = 67$ km s^{-1} Mpc^{-1}. Although these results are not fully consistent

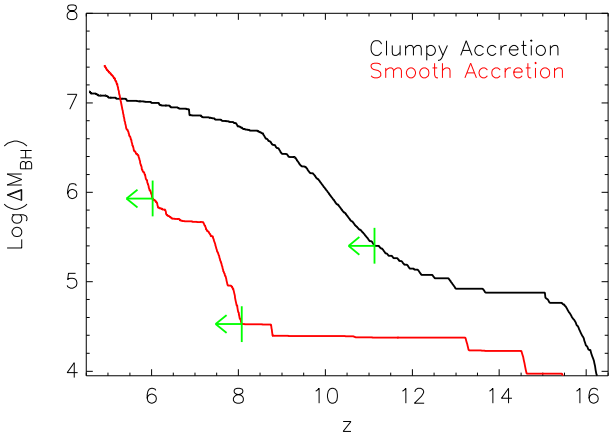

Figure 2. Accreted mass on to our primary black hole in the clumpy-accretion model (black) and smooth-accretion model (red). Green arrows mark the onset of an extended Eddington regime. Black hole mass builds up earlier in the clumpy accretion case, but also leads to a lower final mass.

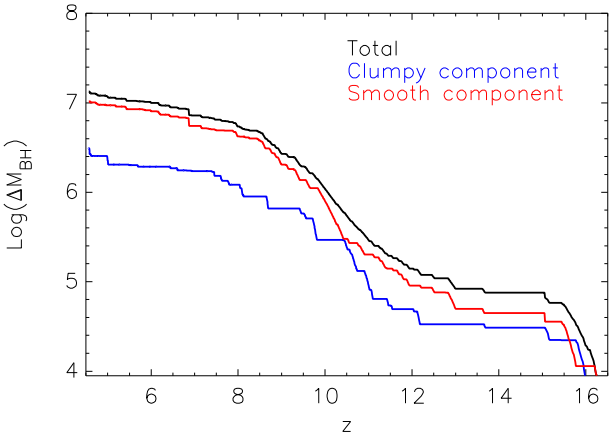

Figure 3. The growth of our primary black hole in the clumpy-accretion model, showing the contribution to the accreted mass from accretion of dense clumps (red) and smooth infall between clump events (blue). The relative importance of the clumpy component of accretion is strongest just as the black hole reaches Eddington at $z \sim 11$.

with the Wilkinson Microwave Anisotropy Probe results (Komatsu et al. 2011), our investigation is based on a comparison of individual objects between two simulation runs, so our results should remain consistent regardless of the exact cosmology used. Within the base 10 Mpc box, we resolve a zoom region of ∼1 Mpc about the largest black hole (based on a low-resolution test run), which reaches $\sim 10^7\,M_\odot$ by $z = 6$. We resolve the zoom region to a maximum physical resolution of ∼76 pc, which corresponds to a refinement level of 17 at $z = 0$. The maximum refinement level at higher redshifts evolves with scale factor (maximum refinment level increase by 1 for each doubling of the scale factor), providing a maximum resolution which remains approximately constant with cosmic time. Refinement is done when a cell contains more than eight dark matter particles, or an equivalent gas mass. Our minimum stellar particle mass is $\sim 4.3 * 10^3\,M_\odot$. Given this base simulation setup, we run the same set of initial conditions (generated with the GRAFIC-2 subroutine, see Bertschinger 2001) using three versions of the code. The ClumpyAccretion run includes our full black hole treatment, including the subgrid model for accretion of high-density clumps described in Section 2.2. The SmoothAccretion run includes black holes, but using the standard accretion model described in Section 2.1. Note that we refer to this model as the SmoothAccretion since it lacks the periodic bursts of accretion caused by unresolved gas clouds, but the black hole accretion rate none the less varies based on the resolved gas properties around it. Finally, the NoBH run is the base run which does not include black holes at all. The primary analysis of all runs was performed with the data analysis toolkit YT (Turk et al. 2011).

3 BLACK HOLE GROWTH

In Fig. 2, we show the accreted mass growth of our primary black hole in both the clumpy-accretion (black) and the smooth-accretion (red) runs, clearly showing a dramatically different growth history. In both simulations, the black hole follows the typical growth behaviour found in cosmological simulations (e.g. Di Matteo et al. 2008; DeGraf et al. 2012a): it undergoes an initial sub-Eddington growth phase, followed by an extended period of Eddington growth, and upon reaching a high enough mass (relative to its host), self-regulation kicks in, dramatically slowing the growth of the black hole. The main difference between the runs is the onset time of the Eddington growth phase, which occurs much sooner in the clumpy-accretion model. In the smooth-accretion model, the sub-Eddington phase is very long-lasting. Without the added accretion from the dense clumps of gas, the black hole takes until $z \sim 8$ to grow massive enough to reach the Eddington regime. In contrast, the clumpy-accretion model reaches the Eddington regime around $z \sim 10$–11, and has already reached the self-regulation regime by $z \sim 8$. This substantial difference is due to the periods of clump accretion providing short time-scale bursts of Eddington accretion during the sub-Eddington regime. In Fig. 3, we divide the total accreted matter (black) from the clumpy accretion run into two components: the accreted mass during clump-accretion events (blue) and in the absence of clumps (i.e. during smooth accretion; red).

From these curves, it appears that the accretion of clumps plays a relatively minor role. However, this conclusion neglects two important factors. First, the total mass gained during clump accretion is not a meaningful quantity, since the majority of growth occurs during the extended Eddington phase. During this phase, the growth is capped at $M_{\rm Edd}$, and thus an incoming clump will not provide any increase in the accretion rate. For this reason, the meaningful quantity to consider is the mass gained via clump accretion prior to the onset of Eddington accretion. Based on this, we see that the black hole has gained approximately half of its mass through clump accretion near the onset of the Eddington phase ($z \sim 11$), demonstrating a significant impact. Even this check underestimates the importance of the clumps, however, as it neglects the exponential nature of the black hole growth. Because the smooth accretion phases depend upon $M_{\rm BH}^2$, modest increases in mass at early times (such as those caused by early clump accretion events) have an exponential impact on the continued growth of the black hole, which is what causes the dramatic differences between the two simulations in Fig. 2. Thus, we note that relatively minor differences at very early times can significantly affect the late-time behaviour of the black hole.

This ability to drive rapid growth at early times may be of significant importance to the seeding mechanisms for supermassive black holes. Using a standard Bondi-like accretion rate, a very low-mass black hole (e.g. a $10^2\,M_\odot$ seed from a PopIII star) will tend to accrete relatively slowly. This can present a problem when attempting to reach the high masses seen in observations (such at the $10^9\,M_\odot$ BH found at $z \sim 7$ by Mortlock et al. 2011). However, the bursts of accretion provided by high-density clouds can produce substantially more rapid growth among small, early BH seeds. Initial tests

suggest that black holes seeded at masses of $\sim 10^3$ M$_\odot$ can still grow to $\sim 10^7$ M$_\odot$ by $z \sim 7$, which will provide more flexibility in the seeding prescriptions used in cosmological simulations.

Furthermore, the early growth of a black hole can be highly sensitive to the seeding prescription, particularly the seed mass. Although the final mass (maintained via self-regulation) may be relatively insensitive to the seeding prescription, the evolution to that final mass may be significantly different. As Fig. 2 shows, a larger mass early on can result in much faster overall growth. For example, using a seed of 5×10^4 M$_\odot$ will take $\sim$2.5 times longer to reach $10^{5.5}$ M$_\odot$ (approximately when our BH reaches the Eddington regime) than a seed of 10^5 M$_\odot$ if we assume Bondi accretion with constant gas properties. However, the clumpy-accretion events tend to occur at the Eddington rate, which depends on $M_{\rm BH}$ rather than $M_{\rm BH}^2$ (see equations 1 and 2), making it much less sensitive to the seed mass. If we assume all the growth is from these bursts at Eddington, the 5×10^4 M$_\odot$ seed will take only 1.6 times longer than the 10^5 M$_\odot$ seed. Although the actual result will be somewhere between these expectations (and also depend on the evolution of the gas properties), this clearly shows that the incorporation of clumpy accretion has the potential to make the black hole growth much less sensitive to the seed mass. A full study of the impact of clumpy accretion on black hole seeding prescriptions is beyond the scope of this paper, but may prove useful for studies attempting to isolate the formation mechanism for supermassive black hole seeds.

4 IMPACT ON HOST

4.1 Morphology

In Fig. 4, we show images of the gas density (top), gas temperature (middle), and stellar density (bottom) of our galaxy in both the clumpy-accretion model (left) and the smooth-accretion model (right). This figure shows the qualitative effect which the clumpy-accretion model has on the environment in terms of general morphology, AGN-driven outflows, and effect on inflowing gas. The redshift was selected to highlight an outlflow process, but we note that other redshifts after the extended Eddington phase are qualitatively similar (see Section 5 for early time comparison). In the density projections, the smooth-accretion model shows a well-defined disc of cold gas has formed without being disrupted. The clumpy-accretion model, however, shows a less well-defined disc which is relatively puffed out in all directions, i.e. has a less-well defined disc plane. More striking than this, however, is the central region of the galaxy, which has been evacuated of dense gas, leaving a substantial void of low-density, high-temperature gas surrounding the black hole. This is more clearly seen in Fig. 5, which shows the gas density profile (solid lines) for the galaxy in both simulations. These profiles show comparable densities above $\sim$1 kpc (though slightly lower density in the clump-accretion model), but a dramatic difference (up to 2 dex) at smaller scales. Note that the highest resolution cells are $\sim$0.1 kpc, so the results at the smallest scales are not well resolved, but the decrease at sub-kpc scales is well within the resolution of the simulation. This clearly demonstrates the ability of the clump-fed AGN to evacuate the gas from the central region of the galaxy, which will necessarily lead to the suppression of the black hole growth (i.e. self-regulation) as well as quench star formation (investigated in more detail in Section 4.3).

The temperature maps in Fig. 4 also show significant differences, with the clumpy-accretion model showing a hot region surrounding the black hole ($\sim$1 kpc, corresponding to the evacuated region), outside of which there are regions of hot and cold gas. In contrast, the disc in the smooth-accretion model remains cool with fewer regions of temperature variation. Outside the galaxy, the clumpy-accretion model produces bubbles of hot gas inflating away from the black hole (similar to radio cavities observed in galaxies), showing clear evidence of AGN-driven outflows. These hot bubbles of outflowing gas are completely lacking in the smooth-accretion model. Consistent with the higher resolution runs of Gabor & Bournaud (2014), despite using a purely isotropic feedback model the outflows are nearly entirely out of plane, though they are not necessarily axisymmetric (see Section 4.3.1 for more details). This anisotropy is purely a result of the local environment, with dense in-plane gas shielding the rest of the disc from the feedback energy, while the relatively low-density out-of-plane gas is effectively driven out. Fig. 4 clearly shows the outflows driven almost exclusively in directions of low-density gas, and also shows that resolved cold, dense clumps effectively block the outflows.

Unlike the gas density and temperature, the stellar morphology is only weakly affected by the clumpy-accretion model. In the bottom panels of Fig. 4, we plot the stellar density maps, which show only minimal difference between the two runs. The stars in the smooth accretion case are slightly flatter/more elongated than in the clumpy case, which has a more rounded stellar component. This is consistent with the general gas distribution (top panels), and is a fairly small effect. More significantly, we see no evidence of the evacuated region at the centre of the galaxy. This is confirmed in Fig. 5, where the dashed lines show the stellar density profile. We find the smooth accretion model has slightly higher stellar densities, but otherwise the *distribution* of stars is largely unaffected by the AGN feedback, down to the smallest scales. Thus, we find, as expected, that the AGN feedback can have a strong impact on the gas, but has no direct effect on the stellar distribution. It can *indirectly* affect the galaxy's stellar mass by suppressing star formation (resulting in the slightly higher stellar densities in Fig. 5), which we investigate in more detail in Section 4.3.

4.2 Gas properties

In addition to the general morphology, we find notable differences in the gas properties within the host galaxy. In Fig. 6, we show the distribution of gas density (top), temperature (middle), and radial velocity (bottom) versus distance from the galaxy centre for all three simulation runs at $z \sim 7.65$, matching Fig. 4. Pixel colour represents the mass of the gas at the given pixel. First, we note that the difference between the smooth-accretion and no-bh runs is quite small. The smooth-accretion black hole heats some of the nearby ($< \sim$3 kpc) gas to higher temperatures than the no-bh case, and there is some outflowing gas driven at slightly higher velocities, but they are otherwise qualitatively similar. The clumpy-accretion model, however, is substantially different. In the density distribution, we see that in the vicinity of the black hole, the very low-density gas ($\sim 10^{-25}$–10^{-26} g cm^{-3} within $\sim$2 kpc, at the bottom left of the panel) has been completely removed in the clumpy-accretion run. At larger radii, this run has extremely low-density gas ($<10^{-27}$) which is completely missing in the smooth-accretion run. This suggests that the bulk of the low-density gas near the black hole was driven away as outflows, and is thus found at larger radii.

The temperature distributions in Fig. 6 show a similar picture. Although the bulk of the very cold (and high-density) gas remains, the majority of inner ($<$2 kpc) cool gas (between 3×10^4 and 10^6 K) has been heated to higher temperatures, and there is significantly more hot gas ($>10^7$ K) at larger radii. This is consistent with the

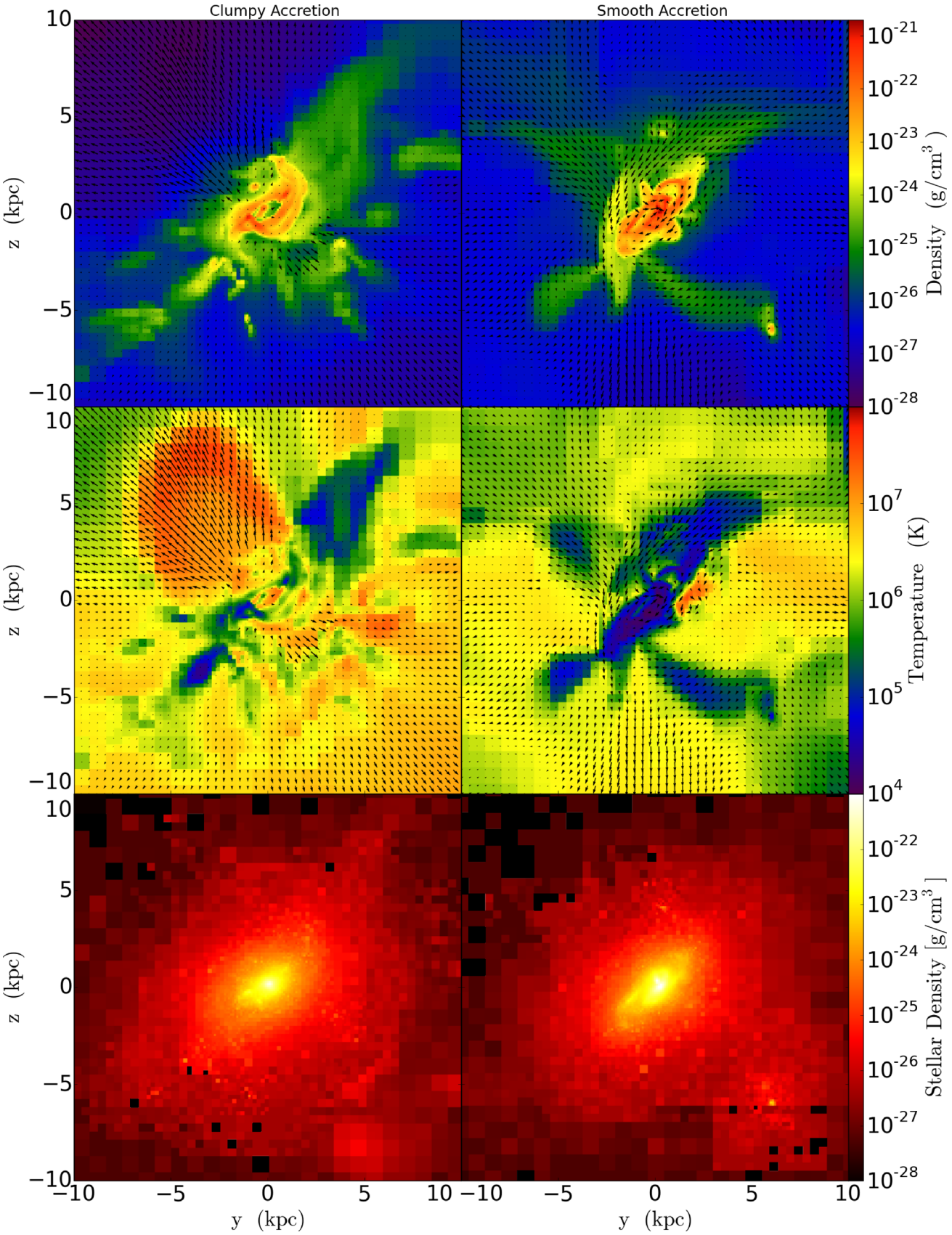

Figure 4. Projected maps of our simulated galaxy at $z = 7.65$ showing AGN-driven outflows in the clumpy-accretion model. Top: gas density; middle: gas temperature; bottom: stellar density. Left-hand panels show the galaxy in the clumpy-accretion simulation; right-hand panels show the galaxy in the smooth-accretion simulation. Each plot is produced from a slice 6-kpc thick. The clumpy accretion has evacuated the centremost region of gas, and drives rapid outflows of hot gas.

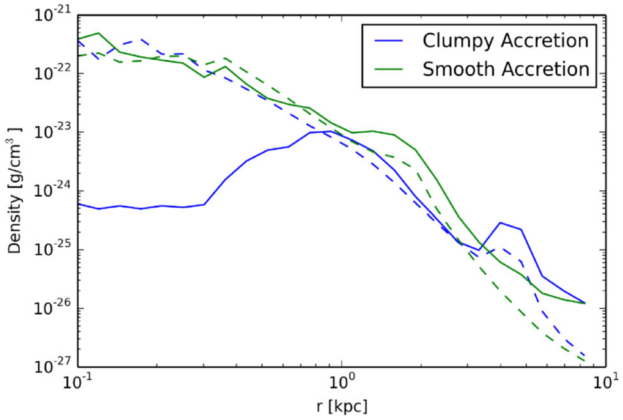

Figure 5. Density profiles for the clumpy-accretion model (blue) and smooth accretion model (green) at $z = 7.65$. Solid lines – gas; dashed lines – stars. Clumpy accretion triggers AGN feedback which lowers the nuclear gas density compared to the smooth accretion case. The stellar profile is minimally affected, with the smooth accretion model having slightly more stars than the clumpy-accretion model.

general picture that the nearby gas has been heated to high temperature and driven out to larger radii. In the bottom panel, we confirm this high-velocity gas outflow driven by the clumpy-accretion black hole, with high velocities (up to 3000 km s^{-1}) maintained out to radii of 8 kpc, compared to the smooth-accretion model where almost no gas exceeds 500 km s^{-1}.

Fig. 7 shows the distribution of gas densities and temperatures as a function of radial velocity. Here, we can explicitly see that the strongly outflowing gas found in the clumpy-accretion simulation is low density ($<10^{-24}$ g cm^{-3}) and high temperature ($>3 \times 10^6$ K, and most above 10^7 K). This is consistent with the high-resolution isolated galaxies of Gabor & Bournaud (2014), who similarly found outflows consisting of hot, diffuse gas. Since none of the strongly outflowing gas is at high densities, we deduce that the AGN-driven outflows do not directly evacuate the star-forming gas, which is dense. Nevertheless, there are other means by which the AGN can suppress star formation, which we investigate further in the next section.

4.3 Inflow and outflow rates

In Fig. 8, we show the instantaneous gas inflow and outflow rates through spherical shells about the galaxy centre. These flow rates are calculated by $\dot{M} = \frac{1}{\Delta x} \sum m_i v_i$, where m_i, v_i are the mass and radial velocity for each cell i in the spherical shell, and Δx is the shell thickness. For thin shells, this is a reasonable approximation. We note that if a sufficiently thin shell is used, the small number of cells contained within it could lead to noisy results. However, despite using very thin shells (only 100 pc thick, comparable to the width of a single cell), the resulting profiles are qualitatively quite smooth, and the results do not depend upon shell thickness. In the smooth-accretion simulation (dashed lines) we find that the inflow rate is nearly an order of magnitude stronger than the outflow rate (except at <1 kpc scales where inflow and outflow are comparable). The exception to this is when a galaxy merger occurs, which provides a localized spike in the inflow rate, often with a corresponding, though much weaker, spike in the outflow rate due to a gaseous component of the infalling galaxy with velocity dispersion or circular velocity larger than the rate of infall. Excluding the effect of incoming galaxy mergers, the inflow rate remains relatively constant outside $\sim$4 kpc scales, below which there is often an increase in both the inflow and outflow rates. In contrast, the clumpy-accretion model can have outflow rates comparable to or higher than the inflow rates if the black hole is large enough (by $z \sim 8$ for this black hole), and the outflows extend out to large radii.

The lack of decrease in outflow rate beyond $\sim$4 kpc suggests two things. First, that the majority of the outflowing gas which reaches $\sim$4 kpc tends to be at or above the escape velocity of the host galaxy (shown to be correct in Fig. 6), and secondly, it suggests that the majority of outflowing gas which reaches $\sim$4 kpc is able to continue outwards without significant retardation by its environment. This is consistent with Fig. 4, which shows that the hot gas tends to expand out of the plane, thereby avoiding the dense in-plane gas which can impede the gas flow. We investigate this directional dependence of the outflows in Section 4.3.1. We also note that the incoming galaxy (seen as a spike in the inflow rate in each simulation) is notably delayed in the clumpy accretion run. This delay is likely due to the hotter gas environment through which it passes. Since the circumgalactic gas tends to have higher outward velocities, the increased ram pressure is able to more efficiently slow the incoming galactic gas.

Although having much stronger outflow rates, Fig. 8 shows that the clumpy accretion run has a generally comparable inflow rate outside the innermost region to that of the smooth accretion run. To investigate the long-term gas inflow on to the galaxy, in Fig. 9, we plot the cumulative gas inflow (blue) and outflow (red) through spherical shells surrounding the central galactic region for both accretion models. This cumulative flow rate is calculated using the instantaneous flow rate at each snapshot, and assuming this rate remains constant until the next snapshot is reached. To avoid having a single thin shell with an unusually high flow rate due to an infalling clump, we take the average flow rate through 10 shells, each 100 pc thick. We show these cumulative curves at radii of 2.5 kpc (top left), 5 kpc (top right), and 10 kpc (bottom left), and a thick-shell curve for flow averaged across all shells between 2 and 10 kpc (bottom right).

Considering the outflowing gas in the clumpy-accretion model (solid red lines), we see that there is significantly more outflow at 2.5 kpc than at 5 kpc, since some of that gas is slowed down by the gas in the galactic disc. At 5 and 10 kpc, however, we find similar outflow rates across cosmic time, confirming that the bulk of the outflowing gas beyond $\sim$3 kpc continues to at least 10 kpc without significant deceleration, consistent with the instantaneous outflow rates in Fig. 8. In contrast to this, the smooth-accretion model (dashed red line) shows a continued decrease in outflowing gas mass out to larger radii. This is expected, since the much lower outflow velocities (see Fig. 8) mean that much less gas from the central region where AGN-driven outflows originate is capable of escaping the potential well, and thus we see the decrease in expelled gas at higher radii.

We also show the cumulative gas infall on to the galaxy (blue), where we again find significant differences between the clumpy- and smooth-accretion models. At early times (prior to $z \sim 8$), we find the gas mass accreted on to the host galaxy is consistent between the two models. This is expected since at early times, the AGN feedback should be insufficient to affect the inflowing gas. Once the black hole is massive enough, however, we note that not only does the clumpy-accretion model provide much stronger outflows, it also substantially suppresses the inflow of gas on to the galaxy, which we see beginning at $z \sim 8$ for this galaxy. Note that at 5 kpc, it appears to start much earlier, but this is due to a high-inflow rate caused by an incoming galaxy in a single snapshot. Ignoring the

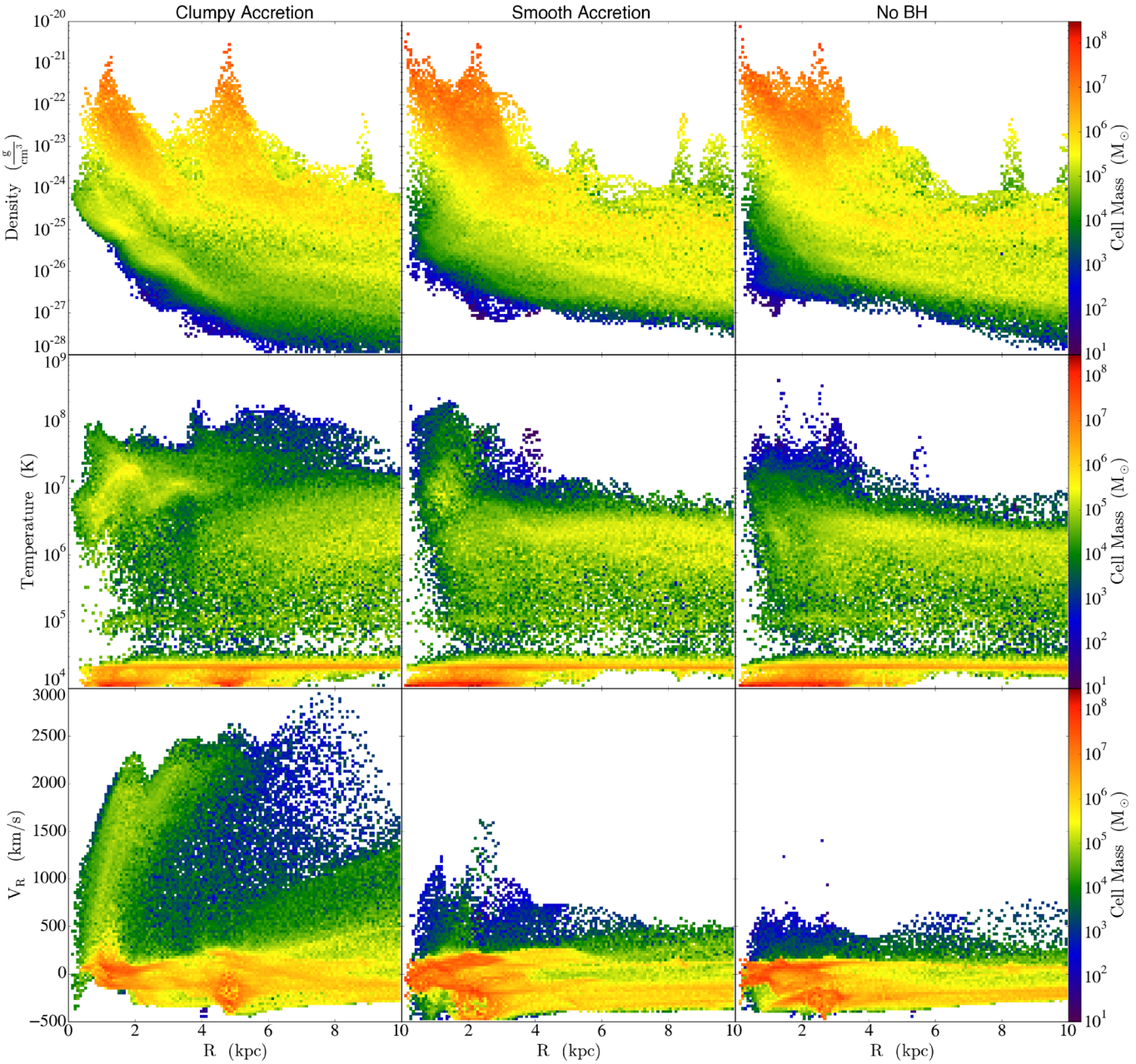

Figure 6. Gas properties of the host galaxy at $z = 7.65$: the density (top), temperature (middle), and radial velocity (bottom) of the gas as a function of radial distance from the galaxy centre for the clumpy-accretion (left), smooth-accretion (middle), and no-bh (right) simulations. Clumpy accretion triggers feedback which heats nuclear gas and drives high-velocity outflows not seen in the smooth accretion or no-bh simulations.

jump caused by this incoming merger, we again see the increased inflow in the smooth accretion case start at $z \sim 8$, also at 5 kpc. This suppression of inflowing gas correlates directly with the onset of self-regulated growth (Fig. 2), suggesting that the regulation of black hole growth is correlated not only with expelling gas from the central region, but also with limiting the replenishment of this reservoir through inflowing gas.

In addition to the flow rates through spherical shells, Fig. 9 shows the cumulative SFR (green lines). Because of the localization of SFR to the high-density regions, we consider star formation within the spherical region interior to the given radius, rather than within a thin shell at the radius. From these curves, we can see that although AGN-driven outflows consist of hot, diffuse gas which does not form stars, the clumpy-accretion AGN none the less significantly quenches star formation by nearly a factor of 2. This appears to be in contrast to the results of Gabor & Bournaud (2014) based on isolated-galaxy simulations, who found that despite driving strong outflows, the star formation rate was minimally affected. However, this apparent discrepancy is due to a difference in the black hole growth phase being investigated, and accounting for this brings both results into agreement with one another. We find that the quenching of star formation occurs only after the black hole has undergone an extended phase of Eddington-limited growth, while the Gabor & Bournaud (2014) investigation used a black hole which is substantially sub-Eddington (except for the bursts due to clump accretion on to the black hole). Compared to their ∼100 Myr simulation in which the black hole only grows by ∼15 per cent (with an averaged Eddington fraction of only a few per cent), we begin seeing

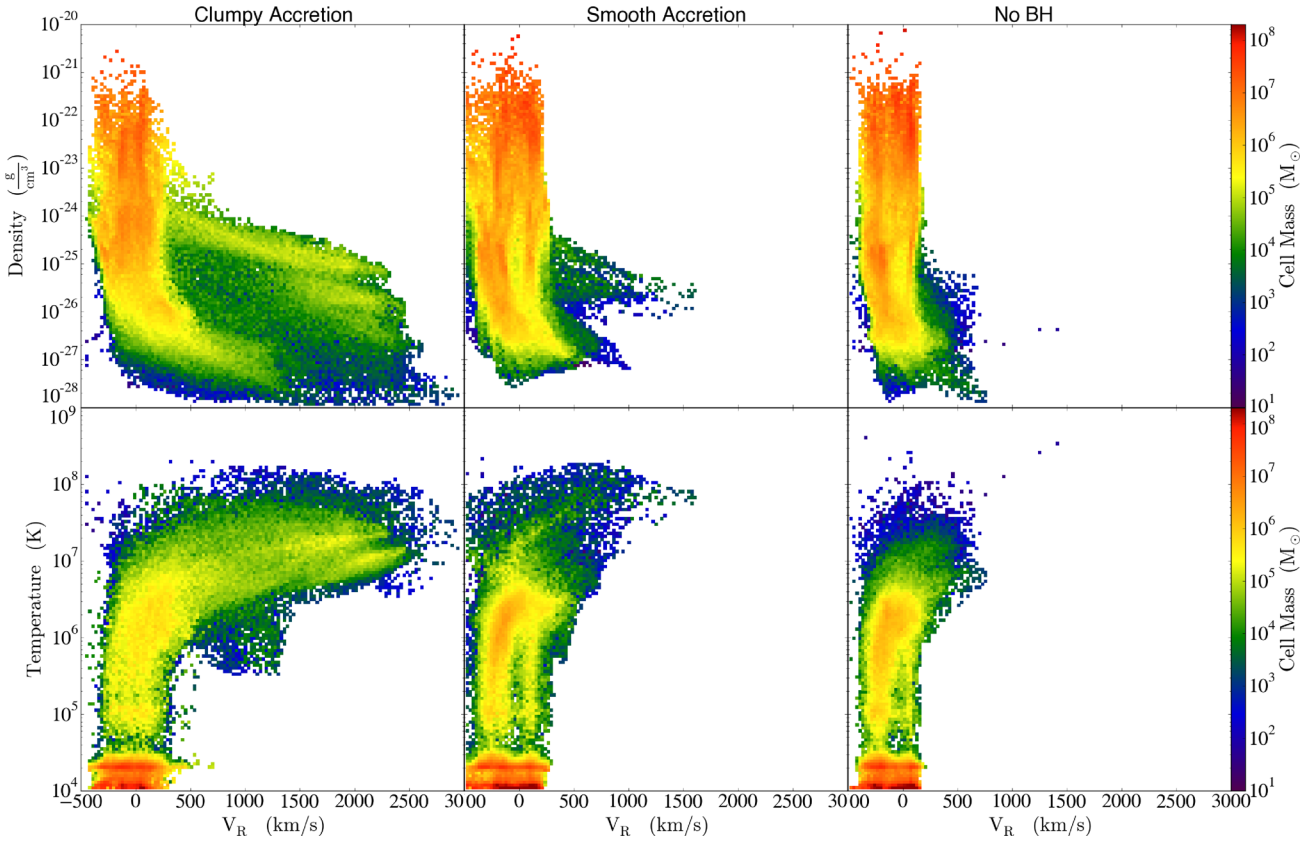

Figure 7. Gas properties of the host galaxy at $z = 7.65$: the density (top) and temperature (bottom) of the gas as a function of radial velocity for the clumpy-accretion (left), smooth-accretion (middle), and no-bh (right) simulations. Clumpy accretion triggers hot, diffuse, high-velocity winds largely absent from the other simulations.

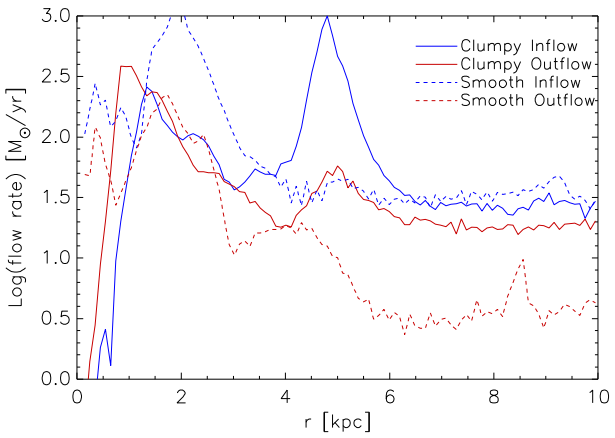

Figure 8. Gas inflow (blue) and outflow (red) rates at $z = 7.65$ as a function of radial distance from the black hole. Clumpy accretion prevents flow into the innermost kpc and drives much stronger outflows out to large scales.

suppression of star formation only after the black hole grows by an order of magnitude at Eddington, and the effect becomes strong only after growing by a factor of ∼40. Prior to such extended growth, we are fully consistent with Gabor & Bournaud (2014): our AGN drives strong outflows of hot, diffuse gas, entraining minimal high-density gas, and being directed almost entirely out of the galactic plane with no significant effect on star formation or host morphology (see Section 5 for more details).

4.3.1 *Geometry of inflows and outflows*

In Fig. 4, we saw that the hot gas driven by the black hole seemed to be strongly directed out of the plane of the galaxy, and in Fig. 8 we saw that the outflowing material did not significantly slow beyond ∼3 kpc, again suggesting expansion away from the dense galactic gas which could impede its progress. To investigate this directly, we compute the radial mass flow as a function of $\cos(\theta)$, where θ is the angle relative to the polar axis of the galaxy. We define the polar axis to be the mass-weighted angular momentum vector of the gas in the central 1 kpc of the galaxy, but we find that these results are not sensitive to the size of the region used to calculate this vector. In Fig. 10, we show the distribution of gas in terms of radial velocity and $\cos(\theta)$, in shells of radius of $R = 2$, 4, 6, and 8 kpc and thicknesses of $0.2R$, for both clumpy accretion (top) and smooth accretion (bottom). Each pixel in V_R-$\cos(\theta)$ is colour coded by the total mass flux through the shell at the given velocity and angle. In the smooth-accretion model, we see that the strongest outflow velocities tend to be out of the plane, but not substantially so, peaking at ∼30° above/below the plane, while the strongest flow rates (rather than flow velocities) tend to be at low velocity and primarily inwards. In the clumpy-accretion model, however, we have a clear angular dependence on the outflowing velocity, with the strongest outflow rates being at the highest velocities, and strongly out of the plane. Furthermore, this clear correlation between outflow velocity and polar angle grows with shell radius, confirming that the more out of plane the gas flows, the less it gets impeded as it travels outwards.

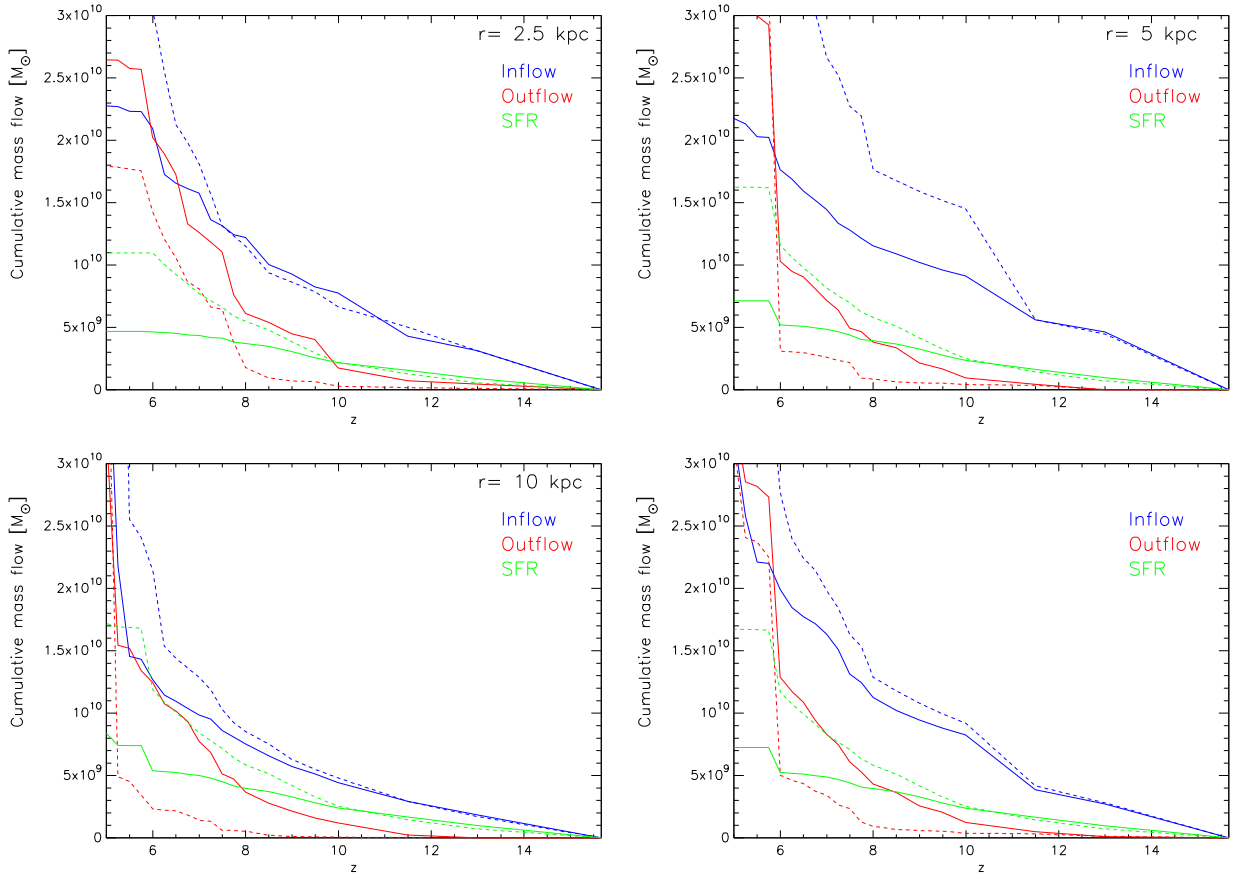

Figure 9. Cumulative gas inflow (blue) and outflow (red) through spherical shells at 2.5 kpc, 5 kpc, and 10 kpc (each 1 kpc thick), and a shell spanning 2–0 kpc as functions of redshift. Also shown is the cumulative SFR (green) in the spherical region interior to the shells. Solid lines show the rates for the clumpy-accretion simulation; dashed lines show the rates for the smooth accretion simulation. Clumpy accretion expels more gas and suppresses both gas inflow and star formation.

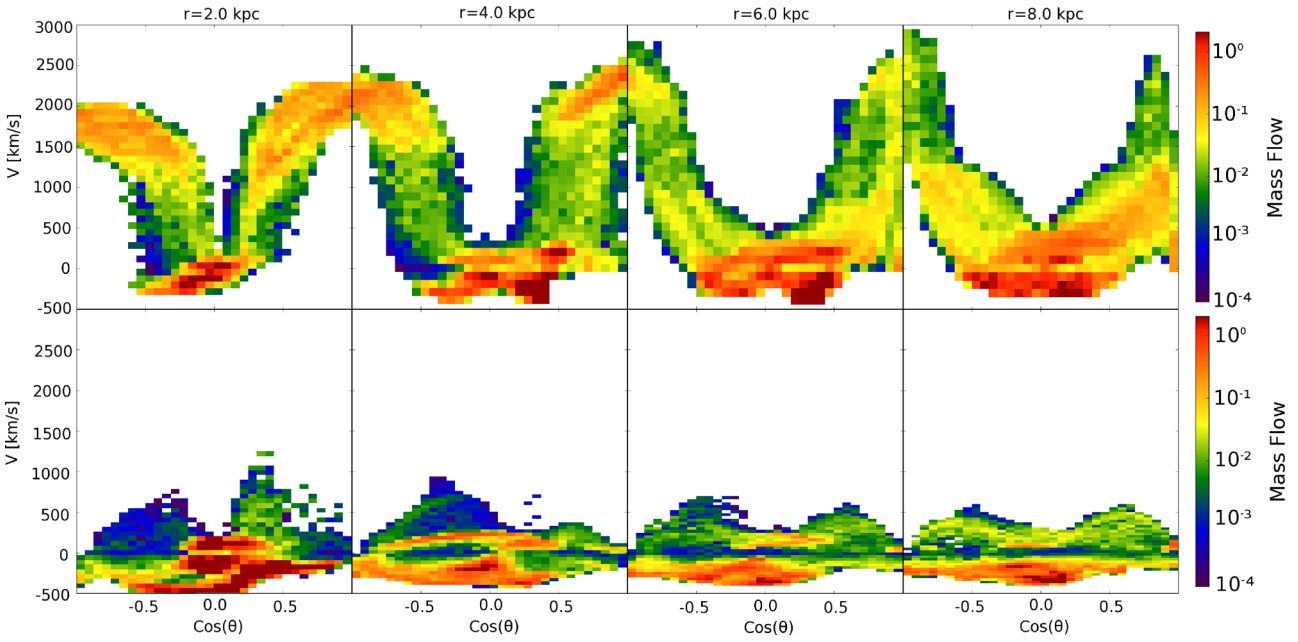

Figure 10. Mass flow rate as a function of radial velocity and polar angle for spherical shells at radii 2, 4, 6, 8 kpc (columns) for the clumpy-accretion run (top) and the smooth-accretion run (bottom) at $z = 7.65$. Outflows in the clumpy-accretion model are directed perpendicular to the galactic plane, particularly at larger radii.

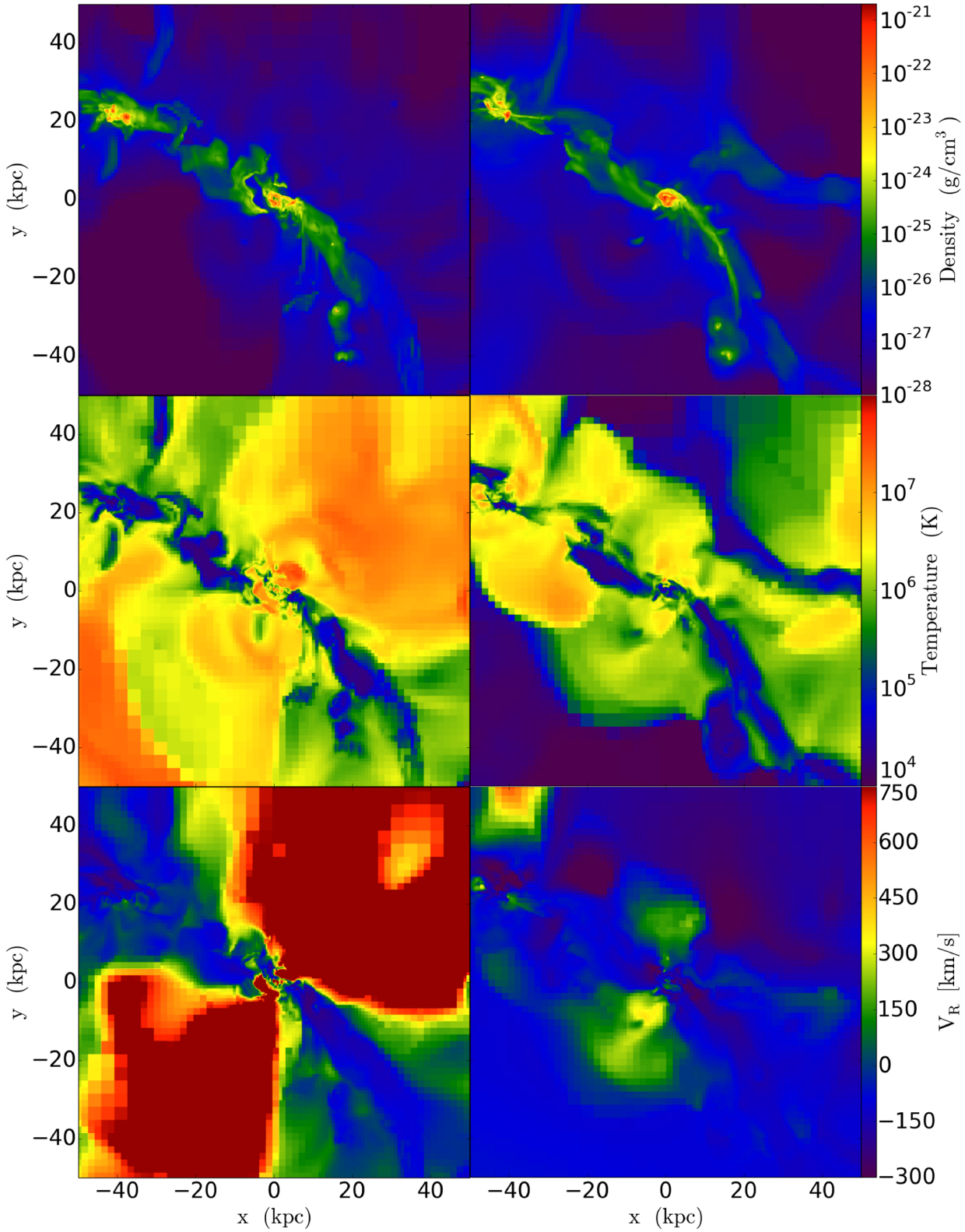

Figure 11. Projection plots of our clumpy-accretion model (left) and smooth-accretion (right) models, showing gas density (top), temperature (middle), and radial velocity (bottom) at $z = 7.65$. Note: to more clearly show the inflow velocities, the radial velocity colour bar is limited to values within [− 300, 700] km.

In contrast to the out-of-plane flows which are relatively unimpeded, the gas moving into the galactic plane is rapidly slowed, with rapid inflow spread over a larger range of θ at large radii (8 and 6 kpc) than small radii (4 and 2 kpc). We also note that in the clumpy-accretion case, at 2 kpc there is outflowing gas directed into the plane (though not as strong as the out of plane), but this outflowing in-plane gas does not survive to 4 kpc. This is due to the void around the black hole (see Fig. 4) which extends to ∼1–2 kpc.

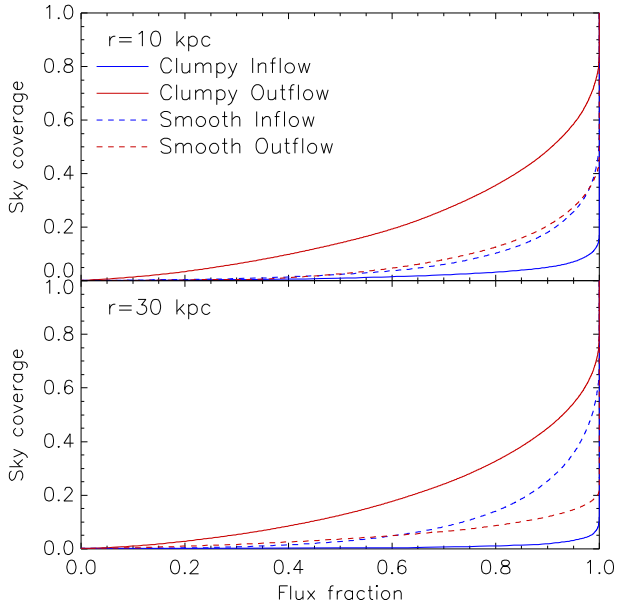

Figure 12. Fraction of sky needed to include a given fraction of the total inflow (blue) and outflow (red) of the gas through a shell at 10 kpc (top) and 30 kpc (bottom) during a period of rapid growth, at $z \sim 8.9$. Compared to the smooth run, outflows from the clumpy accretion run are more widely distributed on the sky, while the inflows are restricted to a smaller covering fraction.

Within the void, in-plane gas flows freely, but is rapidly stopped upon reaching the high-density region. Beyond the void, the only rapidly outflowing gas is that which was directed out of the galactic plane.

4.4 Inflow suppression

In Fig. 9, we showed that the inflowing gas is suppressed in the clumpy-accretion model, showing that the AGN is able to not only drive out hot galactic gas, but affect the inflowing gas streams. In Fig. 11, we show larger scale projections of the gas density (top), temperature (middle), and radial velocity (bottom) to show the means by which the inflow is affected. In the density projections, the smooth accretion model shows more well-defined streams which survive to small scales. In contrast, the inflowing gas streams in the clumpy-accretion model are disrupted by collisions with outflowing gas, most clearly seen by the shock front to the upper-left of the black hole. In addition to the shocks from collisions between the inflowing gas and the outflowing gas, the outer regions of the inflowing gas streams are stripped and blown away, and only the high-density rapidly infalling gas survives. This is seen in the velocity map in Fig. 11 (bottom panels). The colour scale only shows gas with speed below 700 km s^{-1} more clearly shows the variations among the inflowing gas. Here, we see that in the smooth accretion model, the majority of gas is flowing in towards the galaxy (blue), with gradual transition from inflowing to outflowing velocities. In contrast, the clumpy accretion (left) shows relatively small regions where inflowing streams survive.

Furthermore, the inflowing streams completely lack the envelope of more slowly infalling gas seen in the smooth accretion model. Instead, this envelope has been stripped away, leaving a sharp transition between dense, rapidly infalling gas penetrating the rapidly outflowing gas. This stripping effect can also be seen in Fig. 12, which shows the fraction of the sky needed to include a given fraction of the inflowing (blue) and outflowing (red) gas during a period of rapid black hole growth. At ∼10 kpc, the fiducial result from the smooth accretion case shows that inflowing gas and outflowing gas take up comparable fractions of the sky. In the clumpy-accretion model, the outflowing gas is much more widely distributed, with a corresponding compression of the inflowing gas due to the stripping effect described above. At ∼30 kpc, outflow in the fiducial run is compressed to a much smaller fraction of the sky, though note the weaker outflow here means there is very little outflowing gas. Similarly, the clumpy-accretion model again shows substantially expanded outflow comparable to the sky coverage at smaller radii, and compressed inflow.

We note that Dubois et al. (2013a) have also investigated high-redshift black hole growth and the impact on the host galaxy. Similar to our clumpy-accretion model, they found that the black hole is able to evacuate gas from the central galactic region, thereby suppressing star formation, and also reduces gas accretion on to the galaxy. Furthermore, they also found that AGN activity can be driven by dense gas clumps migrating to the galaxy centre (in addition to direct feeding by cold flows), consistent with our general model. However, they tested low- (125 pc) and high- (15 pc) resolution cases, and found that the SFR history was generally consistent between the two runs (except at very high redshifts), contrary to our results presented here. However, we note that their black hole is very efficiently fueled, starting at Eddington upon seeding, and is maintained for an extended period (growing the black hole by two orders of magnitude) due to efficient low angular momentum cold streams. Because these streams are sufficient to maintain Eddington starting from insertion of the black hole into the simulation, we would not expect the resolution of gas clumps to have a significant difference; rather it is in galaxies where the black hole starts at sub-Eddington accretion rates that we expect clumps to have a strong effect as shown here.

5 EARLY-TIME EFFECTS

Although Gabor & Bournaud (2014) found similar outflows (see Section 4.3), neither star formation nor host morphology was significantly affected, seemingly in conflict with the results presented here despite our model being calibrated using that simulation. However, we note that those findings were based upon a short-time-scale (∼100 Myr) run in which the black hole only grew ∼15 per cent (as shown in Fig. 2), and without ever having undergone an extended period of Eddington growth (the only Eddington accretion is found during the 5–10 Myr accretion events). In contrast to this, our simulation predicts that the black hole can impact the host galaxy morphology and star formation rate after having undergone an extended Eddington phase, increasing the mass by more than an order of magnitude.

To provide a more comparable case between the isolated galaxy run and our cosmological runs, we look at the host properties at an earlier time, when the black hole is smaller and has not yet approached the self-regulated regime. Self-regulation occurs at the end of the Eddington regime, where the feedback from the black hole is strong enough to suppress its own accretion. The onset of regulation is where we expect to find the strongest effects, which we showed in earlier sections. To compare with the isolated galaxy, we consider the black hole and its host at $z \sim 10$, when the black hole has reached 10^6 M$_\odot$ but is not yet at the self-regulated regime. In the top panels of Fig. 13, we show the density maps of the host galaxy, finding no significant morphological effects, contrary to Fig. 4, where significant morphological differences were found for

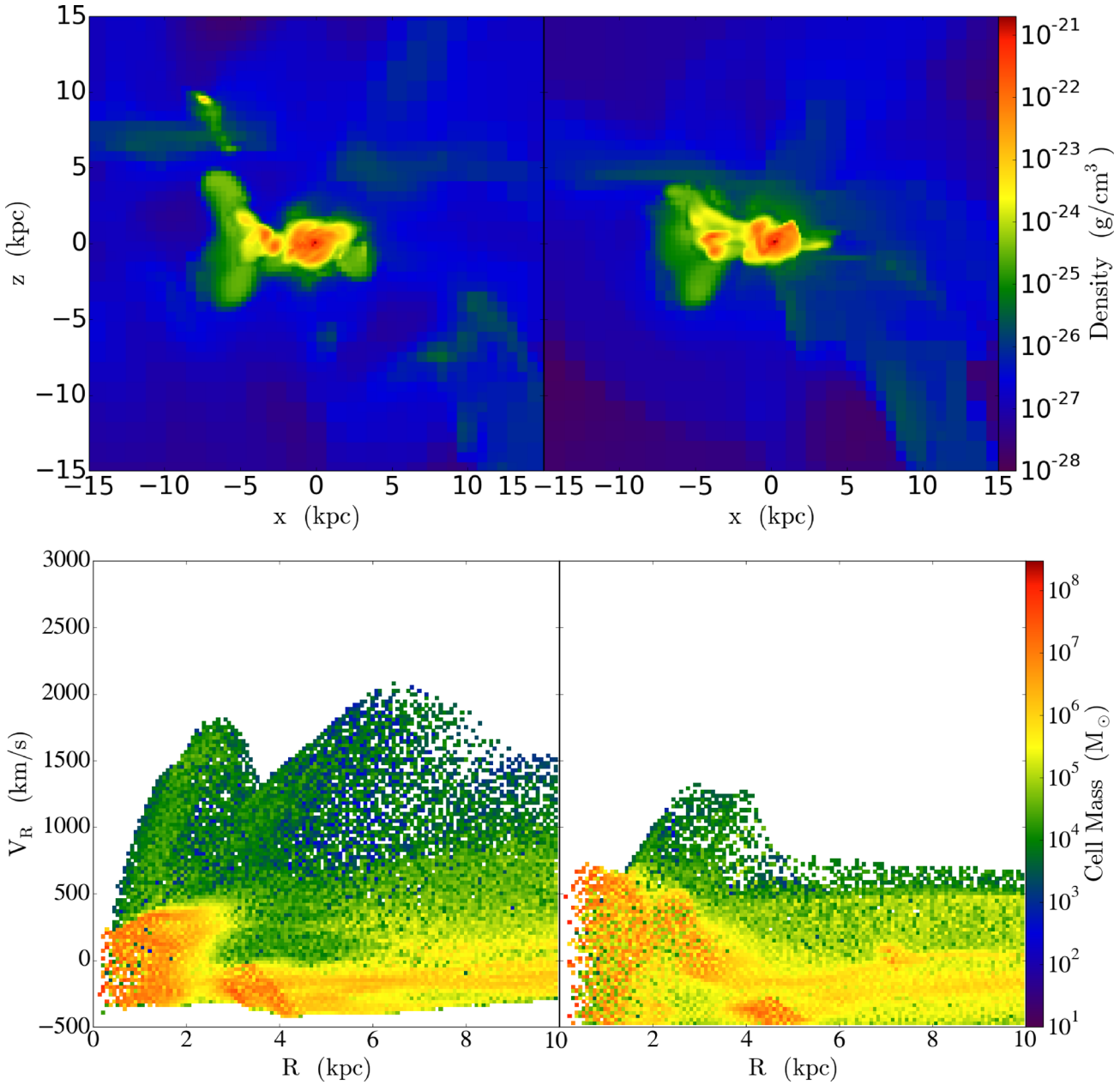

Figure 13. Host galaxy before the black hole reaches the self-regulated regime at $z \sim 10$. Top: density map of gas in 6-kpc-thick slice about the black hole. Bottom: radial velocity distribution as a function of distance from Galactic Centre. Left-hand panels show the clumpy-accretion model, while the right-hand panels show the smooth accretion model. The effect of the clumpy accretion is much weaker than at later times.

the self-regulated regime. In the bottom panel of Fig. 13, we show the distribution of gas velocity as a function of radius, finding that the clumpy-accretion model (left) does drive significantly more gas at much higher velocities than the smooth-accretion model (right). Thus, we find that, consistent with Gabor & Bournaud (2014), if the black hole has not yet undergone significant Eddington growth, it is capable of driving strong outflows of hot, diffuse gas without having a significant effect on the rest of the host galaxy. This is further confirmed in Fig. 9, which shows minimal difference in high-z gas inflow or SFR between the clumpy- and smooth-accretion runs. To quantitatively compare the morphologies, Fig. 14 shows the density profile for both the clumpy- and smooth- accretion models at this early time. The density profiles are in complete agreement, lacking the clear central void in Fig. 5 at the later, Eddington phase. The lack of any such void shows that at early times, comparable to the conditions of Gabor & Bournaud (2014), the black hole has not evacuated the central region, which occurs only after longer term growth and feedback have occurred.

Thus, we find that including periodic accretion of high-density gas clouds can have a strong effect on the host galaxy, but only after the black hole has grown significantly, more than an order of magnitude at approximately Eddington rates. Prior to this growth, the AGN can drive rapid outflows of hot, diffuse gas without suppressing star formation or impacting the overall gas distribution of the host. A further investigation into the impact of periodic accretion bursts should also be performed using a high-resolution isolated galaxy, but one in which a black hole has already undergone extended Eddington growth and is approaching the self-regulated regime. Since

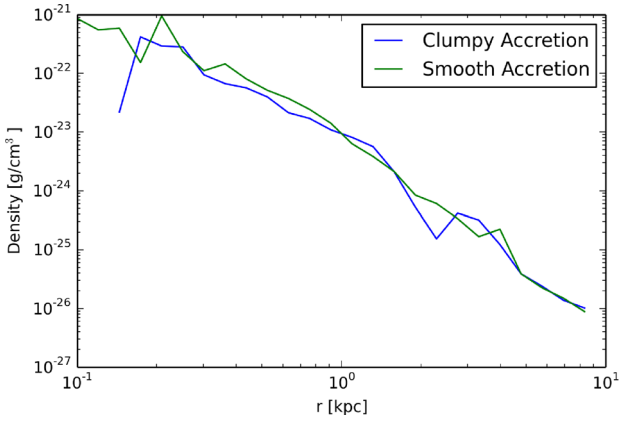

Figure 14. Gas density profile for clumpy-accretion model (blue) and smooth accretion model (green), prior to reaching the self-regulated regime at $z \sim 10$. Clumpy accretion at early time does not affect the gas density of the galaxy.

isolated galaxy simulations cannot be run for such extended times without running into physical limitations (e.g. exhaustion of gas supply in the absence of cosmological inflows), an alternative is to set up initial conditions in which the black hole starts in a very massive state compared to the host, but still in equilibrium. Such simulations are beyond the scope of this paper, so we leave this investigation for a future project.

6 CONCLUSIONS

We find that the increased periods of accretion caused by high-density, small-scale gas clumps is an important factor in the cosmological growth of black holes, affecting both the black hole growth and the impact upon the host evolution.

(i) Inclusion of clumpy-accretion allows for a significant boost to black hole growth starting at early times. Prior to the onset of Eddington-limited growth, although the total mass accreted during these clump phases is comparable to the total mass accreted during smooth phases, the *net effect is much larger*. Because sub-Eddington growth depends on $M_{\rm BH}^2$ (see equation 1), the increased mass due to growth from the clump accretion also serves to increase the accretion rate during the smooth periods, reaching high masses at much earlier times than in the absence of clumpy accretion.

(ii) The increased feedback in the clumpy-accretion model has a significant impact on the host morphology: The central $\sim$1 kpc region about the black hole is mostly evacuated of gas, while at larger radii ($\sim$7–8 kpc), the gas density is higher due to the increased feedback-driven outflows.

(iii) In the absence of clumpy accretion, the inflow is generally an order of magnitude stronger than the outflow beyond the innermost few kiloparsecs. In contrast, the clumpy-accretion model has outflows $\sim 10\times$ stronger, comparable to the inflow rates (excluding incoming galaxy mergers).

(iv) The bulk of the feedback-driven outflows are out of the plane of the galaxy. The feedback energy is deposited isotropically, so the polar outflows are a purely environmental effect, caused by the high-density in-plane gas obstructing in-plane outflows. This effect holds out to large radii, with a tendency for the larger radius outflows to be even more highly collimated.

(v) In the clumpy-accretion model, AGN feedback nearly entirely halts inflow of gas on the $\sim$kpc scale, and at larger scales can suppress gas inflow by nearly a factor of 2. This suppression of inflow has two main causes: the outflows from the galaxy centre directly interact with the inflowing streams and can even stop them; and more generally, the outflows strip the lower density, lower velocity envelope of gas around the high-density streams.

(vi) As a result of the stronger outflows and suppressed inflows, the SFR in the clumpy accretion case can be suppressed by as much as a factor of $\sim$2. However, this difference occurs only after the black hole has undergone an extended period of Eddington growth, growing by at least an order of magnitude. Prior to this extended growth, the SFR remains unaffected.

(vii) Most of the outflow driven by the strong AGN feedback is strong enough to exit the galaxy, without undergoing significant recycling.

Thus, we have demonstrated the importance of incorporating the effects of high-density gas clouds in cosmological simulations, and that applying a stochastic subgrid model to include them can lead to significant changes in host evolution. Having shown the strength this periodicity can have, a more in-depth investigation is necessary to constrain the exact parametrization of the subgrid model. We emphasize that the parameters used here are based upon a single isolated galaxy simulation, and treated as if they hold universally. Although our simulated galaxy does indeed maintain a high enough gas fraction to support our choice of baseline model, it none the less remains an oversimplification. This model was sufficient to demonstrate the importance which dense gas clumps (and variability in general) can have on black hole growth and the corresponding impact on host galaxy evolution, but it does not provide a statistical sample for the relative importance in large populations of black holes. Further high-resolution simulations will be needed to explore the parameter space of potential hosts to determine how the frequency and strength of incoming gas clouds depend upon various properties, including, but not limited to, host mass, gas fraction, stellar mass, disc height, merger history, etc. With a better-constrained set of host-dependent parameters for the bursts of accretion, a full statistical analysis must be done to determine the effect on statistical samples of black holes, including possible observable signatures in the quasar luminosity function and luminosity-dependent clustering behaviour. This continuation goes beyond the scope of this paper and will be addressed in a follow-up work.

ACKNOWLEDGEMENTS

This work was supported by ISF grant 24/12, by GIF grant G-1052-104.7/2009, by a DIP grant, by the I-CORE Program of the PBC, by ISF grant 1829/12, by NSF grants AST-1010033 and AST-1405962, and supported from the E.C. through an ERC grant StG-257720. Some of the simulations used in this work were performed on GENCI resources at TGCC (project 04-2192).

REFERENCES

Begelman M. C., Volonteri M., Rees M. J., 2006, MNRAS, 370, 289
Bertschinger E., 2001, ApJS, 137, 1
Bondi H., 1952, MNRAS, 112, 195
Bondi H., Hoyle F., 1944, MNRAS, 104, 273
Booth C. M., Schaye J., 2009, MNRAS, 398, 53
Bournaud F., Dekel A., Teyssier R., Cacciato M., Daddi E., Juneau S., Shankar F., 2011, ApJ, 741, L33
Bournaud F. et al., 2012, ApJ, 757, 81
Bower R. G., Benson A. J., Malbon R., Helly J. C., Frenk C. S., Baugh C. M., Cole S., Lacey C. G., 2006, MNRAS, 370, 645
Bromm V., Larson R. B., 2004, ARA&A, 42, 79
Bromm V., Loeb A., 2003, ApJ, 596, 34

Burkert A., Silk J., 2001, ApJ, 554, L151
Cattaneo A. et al., 2009, Nature, 460, 213
Ceverino D., Dekel A., Bournaud F., 2010, MNRAS, 404, 2151
Churazov E., Sazonov S., Sunyaev R., Forman W., Jones C., Böhringer H., 2005, MNRAS, 363, L91
Cicone C. et al., 2014, A&A, 562, A21
Ciotti L., Ostriker J. P., 2007, ApJ, 665, 1038
Cisternas M. et al., 2011, ApJ, 726, 57
Coldwell G. V., Lambas D. G., 2006, MNRAS, 371, 786
Croton D. J. et al., 2006, MNRAS, 365, 11
Debuhr J., Quataert E., Ma C.-P., Hopkins P., 2010, MNRAS, 406, L55
Debuhr J., Quataert E., Ma C.-P., 2011, MNRAS, 412, 1341
DeGraf C., Di Matteo T., Khandai N., Croft R., 2012a, ApJ, 755, L8
DeGraf C., Di Matteo T., Khandai N., Croft R., Lopez J., Springel V., 2012b, MNRAS, 424, 1892
Dekel A., Sari R., Ceverino D., 2009, ApJ, 703, 785
Di Matteo T., Springel V., Hernquist L., 2005, Nature, 433, 604
Di Matteo T., Colberg J., Springel V., Hernquist L., Sijacki D., 2008, ApJ, 676, 33
Di Matteo T., Khandai N., DeGraf C., Feng Y., Croft R. A. C., Lopez J., Springel V., 2012, ApJ, 745, L29
Dubois Y., Pichon C., Haehnelt M., Kimm T., Slyz A., Devriendt J., Pogosyan D., 2012, MNRAS, 423, 3616
Dubois Y., Pichon C., Devriendt J., Silk J., Haehnelt M., Kimm T., Slyz A., 2013a, MNRAS, 428, 2885
Dubois Y., Gavazzi R., Peirani S., Silk J., 2013b, MNRAS, 433, 3297
Eddington A. S., 1916, MNRAS, 77, 16
Ellison S. L., Patton D. R., Mendel J. T., Scudder J. M., 2011, MNRAS, 418, 2043
Fabian A. C., Sanders J. S., Taylor G. B., Allen S. W., Crawford C. S., Johnstone R. M., Iwasawa K., 2006, MNRAS, 366, 417
Ferrarese L., Merritt D., 2000, ApJ, 539, L9
Gabor J. M., Bournaud F., 2013, MNRAS, 434, 606
Gabor J. M., Bournaud F., 2014, MNRAS, 441, 1615
Gabor J. M. et al., 2009, ApJ, 691, 705
Gebhardt K. et al., 2000, ApJ, 539, L13
Georgakakis A. et al., 2009, MNRAS, 397, 623
Graham A. W., Driver S. P., 2007, ApJ, 655, 77
Granato G. L., De Zotti G., Silva L., Bressan A., Danese L., 2004, ApJ, 600, 580
Grogin N. A. et al., 2005, ApJ, 627, L97
Haardt F., Madau P., 1996, ApJ, 461, 20
Hernquist L., 1989, Nature, 340, 687
Hopkins P. F., Hernquist L., Martini P., Cox T. J., Robertson B., Di Matteo T., Springel V., 2005a, ApJ, 625, L71
Hopkins P. F., Hernquist L., Cox T. J., Di Matteo T., Martini P., Robertson B., Springel V., 2005b, ApJ, 630, 705
Hopkins P. F., Richards G. T., Hernquist L., 2007, ApJ, 654, 731
Hopkins P. F., Cox T. J., Kereš D., Hernquist L., 2008, ApJS, 175, 390
Hoyle F., Lyttleton R. A., 1939, Proc. Camb. Phil. Soc., 35, 405
Johansson P. H., Burkert A., Naab T., 2009, ApJ, 707, L184
Kawata D., Gibson B. K., 2005, MNRAS, 358, L16
Kennicutt R. C., Jr, 1998, ApJ, 498, 541
Kocevski D. D. et al., 2012, ApJ, 744, 148
Komatsu E. et al., 2011, ApJS, 192, 18
Kormendy J., Ho L. C., 2013, ARA&A, 51, 511
Kormendy J., Richstone D., 1995, ARA&A, 33, 581
Krumholz M. R., Tan J. C., 2007, ApJ, 654, 304
McConnell N. J., Ma C.-P., 2013, ApJ, 764, 184
Magorrian J. et al., 1998, AJ, 115, 2285
Malbon R. K., Baugh C. M., Frenk C. S., Lacey C. G., 2007, MNRAS, 382, 1394
Mandelker N., Dekel A., Ceverino D., Tweed D., Moody C. E., Primack J., 2014, MNRAS, 443, 3675
Mortlock D. J. et al., 2011, Nature, 474, 616
Novak G. S., Faber S. M., Dekel A., 2006, ApJ, 637, 96
Novak G. S., Ostriker J. P., Ciotti L., 2011, ApJ, 737, 26
Planck Collaboration XVI, 2013, A&A, 571, A16
Rasera Y., Teyssier R., 2006, A&A, 445, 1
Rupke D. S. N., Veilleux S., 2011, ApJ, 729, L27
Rupke D. S., Veilleux S., Sanders D. B., 2005, ApJS, 160, 115
Sazonov S. Y., Ostriker J. P., Sunyaev R. A., 2004, MNRAS, 347, 144
Schmitt H. R., 2001, AJ, 122, 2243
Shakura N. I., Sunyaev R. A., 1973, A&A, 24, 337
Sijacki D., Springel V., di Matteo T., Hernquist L., 2007, MNRAS, 380, 877
Sijacki D., Springel V., Haehnelt M. G., 2009, MNRAS, 400, 100
Silk J., Rees M. J., 1998, A&A, 331, L1
Spoon H. W. W. et al., 2013, ApJ, 775, 127
Springel V. et al., 2005, Nature, 435, 629
Stinson G., Seth A., Katz N., Wadsley J., Governato F., Quinn T., 2006, MNRAS, 373, 1074
Teyssier R., 2002, A&A, 385, 337
Teyssier R., Pontzen A., Dubois Y., Read J. I., 2013, MNRAS, 429, 3068
Tremaine S. et al., 2002, ApJ, 574, 740
Truelove J. K., Klein R. I., McKee C. F., Holliman J. H., II, Howell L. H., Greenough J. A., 1997, ApJ, 489, L179
Turk M. J., Smith B. D., Oishi J. S., Skory S., Skillman S. W., Abel T., Norman M. L., 2011, ApJS, 192, 9
Veilleux S. et al., 2013, ApJ, 776, 27
Wyithe J. S. B., Loeb A., 2003, ApJ, 595, 614
Yoshida N., Omukai K., Hernquist L., Abel T., 2006, ApJ, 652, 6

This paper has been typeset from a TEX/LATEX file prepared by the author.